EUROGRAPHICS - IEEE VGTC Symposium on Visualization (2005)
K. W. Brodlie, D. J. Duke, K. I. Joy (Editors)

Analysis and Visualization of 3-C PIV Images from HART II using Image Processing Methods

J. Ebling and G.Scheuermann and B. G. van der Wall[2]

Institut für Informatik, Universität Leipzig, Germany [2] DLR Braunschweig, Germany

Abstract

In this paper, three-component particle image velocimetry (3-C PIV) measurements within the wake of a helicopter rotor from the HART II test are analyzed. These PIV-images are quite a challenge as the noise due to the measurement method and the inherent turbulence of the flow can not be distinguished. Furthermore, features are often hidden by a mean flow, which is influenced by vortices and therefore not easy to determine. The authors present some image processing methods adapted to these vector fields for the computation of position, size, and direction of the vortices in this data. These methods are quite robust in terms of noise and independent of any mean flow and therefore appropriate for this analysis. The results of the analysis allow a more descriptive and intuitive visualization of the vortices.

Categories and Subject Descriptors (according to ACM CCS): I.4.7 [Image Processing and Computer Vision]: Feature MeasurementSize and shape J.2 [Computer Applications]: Physical Sciences and EngineeringAerospace

1. Introduction

In 2001, a major international cooperative research program was conducted to investigate the physics of blade pressure, noise radiation, and vibrations caused by the wake of helicopter rotors [BBvdW*02, vdWBY*]. Concurrently, a comprehensive experimental database for code development and validation has been generated. There are three major sources for blade pressure fluctuations, noise and vibrations – the superposition of flight speed and blade rotation, the aerodynamic interference between the rotor and the main body of the helicopter, and the wake vortices of the rotor hitting other blades. This research program concentrates on the latter phenomena. It is called HART II for Higher-harmonic-control (HHC) Aeroacoustics Rotor Test II and it is a follow up on the HART program of 1994. (HHC describes the process of influencing the blade pitch angle, 3,4 or 5 times per revolution reduce noise and vibration.) The German DLR, the French ONERA, the Netherlands DNW, the US Army Aeroflightdynamics (AFDD) and NASA Langley all take part in the cooperation.

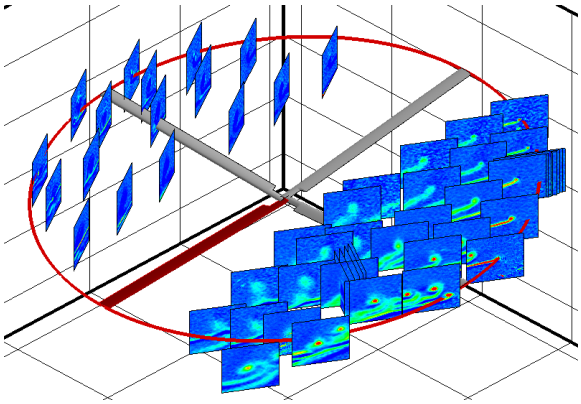

Figure 1: *PIV measurement positions in the wake of a helicopter rotor. The red blade is at the rear position, and the wind comes from right. Figure courtesy of DLR Braunschweig.*

Part of the measurements were so called three-component particle image velocimetry (3-C PIV) measurements, which resulted in three-component vector fields of the flow measured in image planes (Figure 1). There are immediately two challenges concerning this data. First of all, the velocity of the particles in the major flow direction is often, though not

always, much bigger than the vortex components and thus hides the vortices. Furthermore, the data has been measured and therefore contains measurement error besides the natural turbulence of this flow. An analysis of the size of the errors of the PIV measurement can be found in [RRE*04]. Most of the time, the vortices are not orthogonal to the measurement plane. Methods for determining, for example, the size of the vortices will therefore give biased results. It is necessary to determine the direction of the vortex and to correct the data by projecting the (three-component) vectors onto a plane orthogonal to the vortex. There is often more than one vortex in the data and the vortices and the wake sheet can influence each other, resulting again in a non-optimal vortex shape in the image plane. Every vortex has to be found and corrected separately by removing the influence of other vortices, which is a recursive problem.

Image processing is a mature field and methods like convolution are widely used which are robust in terms of noise. Convolution and Fourier transform have recently been extended quite successfully to vector fields [ES03, ES, HEWK03]. Therefore, convolution based methods are obvious candidates for vortex detection and classification, especially as the data is aligned on a uniform grid. In this paper, the authors show how to address the vortex detection and classification in this data within an image processing framework and give a novel algorithm for determining the orientation of the vortices.

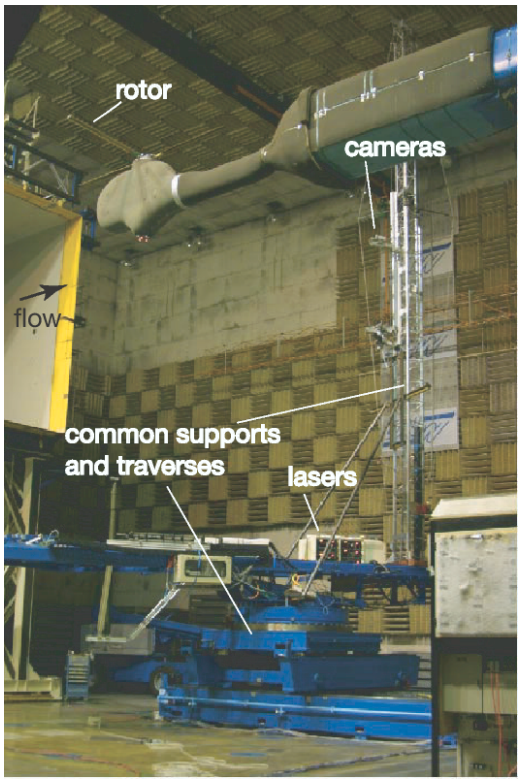

Figure 2: *HART II measurement configuration. Figure courtesy of DLR Braunschweig.*

2. HART II - Test Description

2.1. The Test

The HART II test was conducted in the open-jet, anechoic test section of the Large Low-speed Facility (LLF) of the DNW. The set-up for the PIV measurements is shown in Figure 2. The rotor is a 40-percent, dynamically and Mach-scaled model of the Bo105 main rotor and operated counter clockwise when looking from above. The model is 4m in diameter and has four hingeless blades with a precone of 2.5° at the hub. For the HART II test, the rotor was operated at a nominal rpm of 1041, thrust coefficient C_T=0.0044, hover tip speed of 218m/s, and an advance ratio of 0.15, for a range of rotor angles and conditions with and without HHC. More detailed information can be found in [BBvdW*02, vdWBY*].

2.2. 3-C PIV Measurements

The rotor wake was measured on both the advancing and retreating sides of the rotor using 3C-PIV. The measurement locations (cut planes) are shown in Figure 1. Two rotor azimuthal orientations were used in order to keep the blade from interfering with the measurements. There were approximately 50 locations on each side of the advancing and retreating sides for the baseline and two HHC conditions. For some locations on the advancing side, PIV measurements were made for six different shaft angles to get more precise information about various flight conditions from steep climb to steep descent. At every PIV measurement location, 100 instantaneous vector fields were obtained, not to get time-dependant behaviour, but to average the results to get a statistically based mean behaviour at the positions. The time-dependant behaviour can be studied by tracing the vortices through the different measurement positions as these are placed along the path of the vortices.

The PIV setup for the HART II test consisted of five digital cameras and three double pulse Nd:YAG lasers. The lasers and cameras were mounted on a common traversing system in order to keep the distance between the cameras and the light sheet generated by the lasers constant, even when moving to different measurement locations (Figure 2). Thus, measurements could be continued without recalibration. The five cameras were located on the tower and the lasers underneath the rotor. To obtain measurements on the retreating side, the entire support structure and tower was repositioned.

The three laser systems generated a light sheet of 1.5m, 7mm thick, with an orientation of 30.6° with respect to the wind tunnel axis. The cameras and lasers were synchronized with a one-per-rev signal given by the rotor, allowing for

recording at desired phase-angles of the rotor blade. One camera was used for visual checking of the seeding of the particles in the flow prior to the PIV data acquisition to guide the other cameras to the vortex center. The other four cameras were used for two simultaneous PIV measurements of the overall flow and a small, higher resolution image focused on the vortex core region. Each camera had a resolution of 1024 by 1280 pixel, digitized to 12 bit. One camera from each system was located above and below the rotor plane, respectively. The difference in spatial resolution was obtained by using different lenses.

Flow seeding was accomplished by a specially designed seeding rake located in the settling chamber. The rake was 3m by 4 m and was connected to Laskin nozzle particle generators. Di-2-Ethylhexyl-Sebacat (DEHS) was used as seed material. The mean diameter of the particles generated was below 1 μm. For more detailed information, see [BBvdW*02, BBvdW*03, RRE*04, vdWBY*].

3. Previous Work

3C-PIV measurements have been applied before, and not only to the HART II data. Some measurement of the wake of a hovering helicopter, for example, can be found in [HYWL00], as well as first attempts of processing the vector fields.

3.1. Previous processing of the HART II PIV data

The rotor wake contains vortices in all creation, aging and destruction phases, the destruction being due to bursting or interaction with blades. Regarding direct visualization, the vortices are often hidden by mean flow components (Figure 3 and 7). Removing the mean flow is not as simple as averaging the vectors and subtracting the result as the vortices influence the average. To be independent of the mean velocity components, the out-of-plane component of vorticity ω_z, that is, the vorticity of the two in-plane components, has been used mainly for vortex detection and classification.

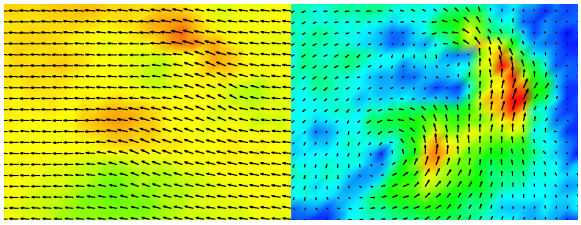

Figure 3: *Hedgehog and colormap of the velocities of the same part of one dataset. Original data (left) and the data after removing the average vector of the field (right). The color map is scaled from zero to the maximal velocity of the data, that is 36.3 for the original data and 11.4 for the data with the average removed.*

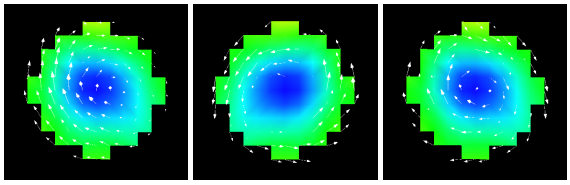

Figure 4: *Part of a 3-C PIV image around a vortex. The global average has already been removed. Left: Velocity in the direction of the vortex. The image is shown from front. Middle and Right: The local average has been removed, too. Now the vectors are only orthogonal to the vortex direction. As the vortex direction is not orthogonal to the image plane, the vectors come out of the plane. The image is shown from front (middle) and back (right).*

Figure 7 shows the vorticity of one of the instantaneous data sets and the effects of measurement errors. In [BBvdW*02], the vortex core is defined as the center of vorticity (CoV),

$$CoV = \frac{\sum_i p(i) * \omega_z(i)}{\sum_i p(i)},$$

where $p(i)$ denotes the position and $\omega_z(i)$ the out-of-plane component of vorticity. The sum is either taken over the whole frame or only within a region around the suspected vortex center, which can be found by manual inspection or locally extremal vorticity. The latter approach has the advantage that the CoV is only influenced by one vortex, but the general area of the vortex and the size have to be determined beforehand.

There are two methods to determine the size of the vortices so far [BBvdW*02, vdWBY*, HYWL00]. First, velocity cuts through the vortex can be analyzed, but these are quite ragged due to the noise. Better results are obtained by integrating the vorticity within a disc that is successively enlarged and plotting the results as a function of the radius. The maximal integration result, divided by the radius, gives the size of the vortex, and the profile, if convex, gives the velocity at the core radius and the parameter N of the Vatistas vortex model [Vat98],

$$v(r) = \frac{v_c r}{(r_c^{2N} + r^{2N})^{1/N}},$$

as described in [BBvdW*02]. For N=1, the Vatistas model equals the Scully vortex model [Scu75] and for $N = \infty$, the Rankine model [Ran58] is obtained.

A problem is the fact that the vortices are not orthogonal to the light sheet where the data is acquired. The angle between vortices and measurement plane can be in the order of 45° or even more [BBvdW*03]. In the images, this presents itself in an elliptical instead of circular shape of the vortices. For a proper evaluation of these vortices, the direction of the vortices has to be determined and the images projected onto

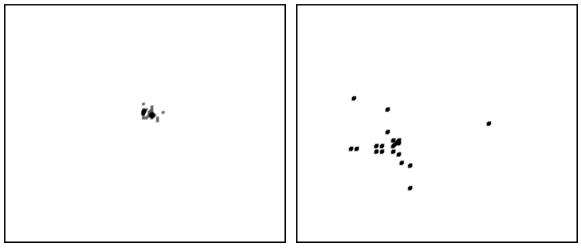

Figure 5: *Vortex core positions at two measurement positions, 20 images each. The measurement position of the left image is shortly after vortex creation and the measurement position of the right image is at a place where the vortex is quite old.*

a plane normal to the vortex direction. Otherwise, for example, the computed size of the vortices will be larger than the actual size.

Two approaches for determining the orientation are described in [BBvdW*03]. The first approach is to remove the mean vectors from the data. Then, within the vortex, averaging of the vectors results in the direction on the vortex as the rotational parts of the vectors erase each other. This approach has to be combined with projecting the data onto the computed orthogonal image plane and iterating the whole process to give good results.

The second approach is to plot the up-wash angles given by the out-of-plane component of the vectors and fit the results with a sine-wave. The maximal value and the zero-crossings of the sine-wave give two angles which determine the direction of the vortex.

Both methods suffer from the fact that the measurement error is largest first in in the vortex core due to less seeding within, and secondly the out-of-plane component itself can not be determined as well as the in-plane components. The averaging of the first method and the fit of the sine-wave in the second method counterbalance some of the errors. Nevertheless, some uncertainty is to be expected. In [RRE*04], it is shown that for well-formed vortices, both methods result in generally the same direction, but in the early stages of formation, the second method is more stable as the relative magnitude of the axial velocity is smaller.

The images at each measurement position were averaged after aligning the vortex core positions as the positions differ due to fluctuations in the rotor tip positions (Figure 5). In some extraneous images, the vortex was not defined well enough, so images where the maximum vorticity ω_z does not exceed a certain threshold are discarded.

3.2. Image Processing on Vector Fields

An obvious approach to image processing of vector fields is to decompose the field into its components for subsequent independent processing using known tools such as convolution and the Fourier transform. Granlund and Knutson [GK95] have investigated this approach in 2D. They also presented the orientation tensor for rotation invariant matching on scalar fields, provided that the scalar fields change only in one direction in the neighbourhood of the matching. This orientation tensor is defined as

$$OT(x) = \sum_{k=1}^{n} f(h_{n_k}(x))(\alpha\, n_k n_k^T - \beta\, I),$$

where n_k are the directions of one rotated filter, $h_{n_k}(x)$ is the similarity of the rotated filter with direction n_k and the field at position x, and f is a function weighting the directed similarity values. In 2D, the minimal amount of directions for mathematical perfect direction calculation is three and the directions are given as

$$n_1 = (1,0)^T,\ n_2 = (a,b)^T,\ \text{and}\ n_3 = (-a,b)^T$$

with $a = 0.5$ and $b = \frac{\sqrt{3}}{2}$. Similarity to a pattern can be computed in image processing with the help of a convolution or a correlation. Convolution is defined as

$$(h * f)(x) = \int_{\mathbb{R}^n} h(x')f(x-x')dx'$$

where h is the pattern to be found, f is the field and x the position where the similarity is to be computed. Actually, Similarities are computed by correlations

$$(h \star f)(x) = \int_{\mathbb{R}^n} h(x')f(x+x')dx',$$

but every correlation can be computed by a convolution with a mask that has been reflected at the center of the mask, and vice versa.

A definition of convolution on vector fields directly can be done by using the generalized inner product of pertinent vectors. Heiberg et al. [HEWK03] define convolution on vector fields using the inner (or scalar) product of two vectors as

$$(\mathbf{h} *_s \mathbf{f})(\mathbf{x}) = \int_{E^d} \langle \mathbf{h}(\mathbf{x'}), \mathbf{f}(\mathbf{x}-\mathbf{x'})\rangle d\mathbf{x'},$$

where $\mathbf{f}$ is the normalized vector field and $\mathbf{h}$ is the filter. The scalar product provides an approximation to the cosine of the angle between the direction of patterns present in the vector field and the direction of the filter. Heiberg et al. do not formulate or use a Fourier transform in their method but they also make use of the orientation tensor for rotation invariant matching in vector fields. Note that the connection of correlation and convolution is similar to the scalar case [ES].

In [ES03], the authors proposed a unified notation for the convolution of scalar and vector fields based on Clifford Algebra and presented the corresponding Fourier transform in [ES]. The convolution presented by Heiberg et al. [HEWK03] is part of this Clifford convolution as the multiplication of two vectors results in an inner (or scalar) and outer product of these vectors in Clifford Algebra. For this paper, not all of the properties of Clifford convolution are

explicitly needed and therefore the authors will stick to the definition used by Heiberg et al. [HEWK03], but the reader should remember that any following analysis will most likely need Fourier transform and the unified convolution notation and that the change to Clifford convolution is easy.

4. Image processing methods on the HART II data

4.1. Detecting the Vortices

To detect vortices with the use of a convolution, a vector valued mask describing the vortex can be used. Masks that have been successfully used are a pure rotation and a Rankine vortex as shown in Figure 6. An example of a similarity image thus computed can be found in Figure 7. Note that it is quite similar to smoothing of a vorticity field. The masks shown in Figure 6 are rotational symmetric. Therefore, it is enough to compute one convolution only in order to get a rotational invariant similarity. Furthermore, the masks have zero mean and thus they are not affected by any mean flow (Figure 7). This is, as stated previously, important for the analysis of this data.

This far, the similarity values are only given at the nodes of the grid. To get subpixel accuracy, the authors propose two different methods. Similar to the CoV, the center of similarity (CoS),

$$CoS = \frac{\sum_i p(i) * s(i)}{\sum i p(i)},$$

where $p(i)$ denotes the position and $s(i)$ the similarity values, can be computed. CoS and CoV results in exactly the same positions. To determine the neighbourhood before the CoS computation automatically, the authors propose to first approximate the size of the vortex, without subpixel accuracy. The region thus defined, or a multiple, can be used before the computation of CoV or CoS.

Another approach is to use a kind of bisection method. Note that linear interpolation, which is most often used in grids, can be computed via a convolution with an triangle filter and that (scalar) convolutions are commutative. That means that computing the similarity at an arbitrary point in a cell of the grid results in the same value as computing the similarity at the nodes and then interpolating the results. Thus, the maximal similarity can only be at a grid node. However, masks can be generated with the rotation center at every arbitrary point in space. So, the mask is not moved for subpixel accuracy, but the vortex core or rotation center within the mask. It has the disadvantage that the mask has to be computed for every new position but the similarity values of different subpixel positions are nearly equal within a few iterations. This bisection methods needs less data than CoS, but if the neighbourhood for the CoS computation is large enough, the bisection method is not as precise.

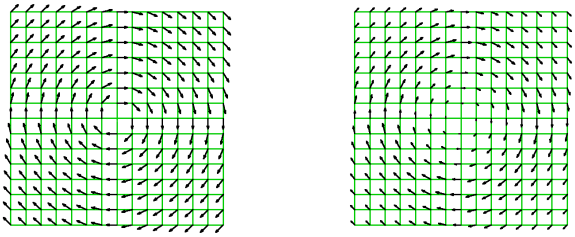

Figure 6: *A normalized rotational mask (left) and a Rankine vortex mask (right).*

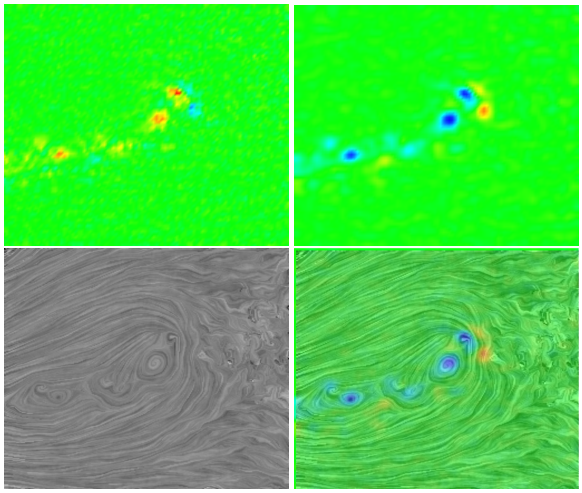

Figure 7: *Top: Vorticity (top left) and a similarity image (top right). The similarity to a 5^2 rotational mask is shown where blue denotes high similarity to a lefthanded rotation and red a high similarity to a righthanded rotation. Therefore the color is inverted in comparison to the vorticity image. Note that the scaling differs, between ± 4500 in the case of vorticity and ± 4 for the similarity image. Bottom: Line integral convolution (LIC) of the field where the average has been subtracted (bottom left) and LIC overlaid with the similarity image (bottom right).*

4.2. Determining the Size

When the grid node with (locally) maximal similarity has been determined, the size of the vortex can be found by using successively larger masks (Figure 8) at the position of the vortex center until the similarity values begin to drop off (Figure 9). Note that the vortices are assumed to be circular, at least after orientation correction. The scale analysis can as well be used with masks having the vortex center at a grid point or with masks which have the vortex center at the subpixel position. There is not much difference in the results of those masks due to the averaging effects of convolution.

When the vortices in the image plane have an elliptical

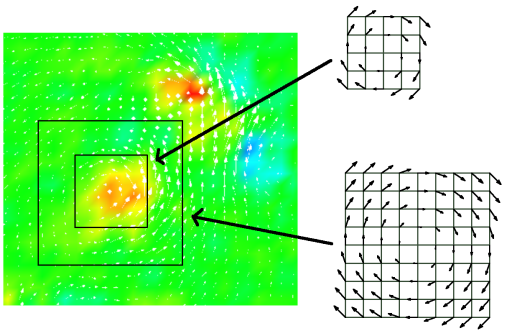

Figure 8: *The size of a vortex can be determined by convolution with successively larger masks.*

shape because their orientation has not yet been corrected, the detection of the vortex with a smaller mask can give wrong results (see isolines in Figure 11). Then, the computation of the scale should be done within a small region of the assumed vortex center. The region can be detected automatically by using all positions in the neighbourhood which have similarity measures above a certain percentage of the maximal similarity value. There is a relationship between computational effort and a stable threshold, but the regions are not that large and, for example, 33% gives stable results for all datasets tested. The position which gave the largest similarity in the computation of the scale of the vortex is the grid node next to the true vortex center and determines the scale of the vortex. This position is not automatically the position with maximal scale as can be seen in Figure 9. Note that it is not sensible to use subpixel accuracy before the grid node next to the true vortex center has been identified.

Again, the scale is only determined with an accuracy of

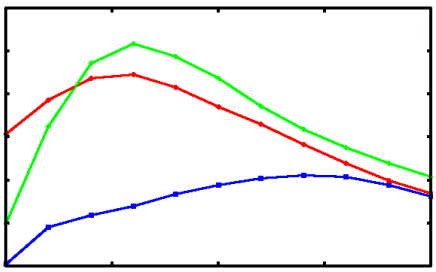

Figure 9: *Similarity with a pure rotational mask (y-axis) vs. mask size (x-axis) for three positions. Shown are the position with maximal similarity to the 5^2 rotational mask (red), the mask with maximal similarity within the scale computation (green), and the position with maximal mask size within the region defined by a percentage threshold (blue). The maximal similarity of the green line determines the position and size of the vortex.*

edge length so far. For subpixel accuracy, the trick from the last subsection has to be used again. Here, this means that the size of the mask stays the same but the assumed core radius is changed. This way, an accuracy of one tenth of the edge length can be achieved. A pure rotational mask is no longer optimal. The Rankine mask itself behaves not bad, but for subpixel accuracy, the velocity at the core radius should be enlarged to get a significant drop-off in the similarity values once the radius is bigger than the vortex core radius. Another possibility is to use only the vectors within half an edge or less of the core radius and zero the rest. With this mask, the velocity at the core radius v_r can be read of directly from the similarity values. Because of the averaging, the result is a little bit smaller than the actual values, but not significantly so.

4.3. Orientation Correction

Looking at Figure 10 and 11, the idea for the determination of the vortex direction can be explained quite well. First of all, it is assumed that position and size of the vortex are known, though not necessarily with subpixel accuracy. Then, a local coordinate system with origin in the vortex center is used. The direction of the major axis of the ellipse has to be aligned with the local x-axis. The rotation angle around the local out-of-plane axis (z-axis) can be computed quite easily out of the direction of the major axis. Then, the plane itself has to be tilted. The angle for this rotation is given by the arc cosine of the ratio of the size of the major and the second axis of the ellipse. The last step is to determine the direction of the tilt - positive or negative.

This method is based on the assumption, that the vortices are perfectly circular. In practice, this is not always the case. Especially in the early stages of vortex creation, elliptical or band-shaped vortices have been observed. Nevertheless, for most of the measurement positions of the HART II PIV images, this assumption is warrantable.

A tensor is optimal for describing ellipsoids. Thus, the authors now use the orientation tensor in combination with the convolution. Then, the major axis of the ellipse is given by the first eigenvector and the ratio of the two axes by the two eigenvalues. To determine the sign of the tilt, the vectors

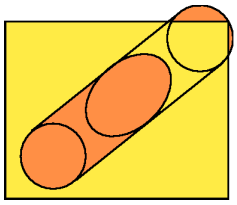

Figure 10: *When the direction of the vortex is not orthogonal to the image plane, the vortex shape in the image plane will be elliptical.*

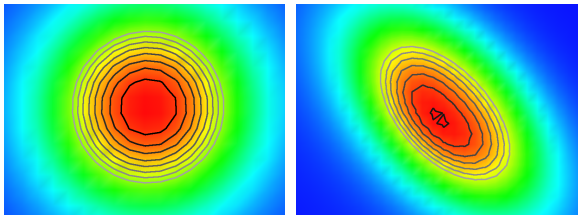

Figure 11: *Looking at similarity images gained by convolving a data set with a rotational mask or a Rankine vortex, the shape of the resulting image tells whether the vortex direction is orthogonal to the cutting or image plane (left) or not (right). Out of the shape of the ellipse in the right image, the direction of the vortex can be computed except for the sign of the second rotation angle. The color map of the similarity image, where red denotes high similarity and blue low similarity, is overlaid with isolines.*

itself have to be used again. Here, the authors propose to subtract the total average and then average the vectors within the vortex region. Then, the sign of the y-component of the result gives the sign of the tilt.

One idea was to determine the shape of the ellipse out of isolines as shown in Figure 11. But because of the noise, the actual isolines in the HART II PIV images are quite ragged and thus transport the noise into the results. Therefore, elliptical masks are used which can also be interpreted as an integration of several isolines.

Now, which mask gives the best results? First of all, the authors tried an elliptical Rankine vortex with ratio 1:2 in combination with the orientation tensor. The size of the larger axis was chosen as the diameter given by the approximated size of the vortex. The next idea was to use a circular Rankine vortex or a simple rotational mask with half the approximated scale. These resulted in a similarity image similar to Figure 11. On this scalar-valued similarity image, convolutions with a scalar-valued, elliptical mask, which has the same shape as the vector-valued elliptical mask of the previous method, was performed and combined with the orientation tensor.

The second approach gave slightly better results as the form of the ellipse was not as restricted as for the vector-valued elliptic mask. Furthermore, the scalar similarity image is pretty smooth which might be the second reason for the better behaviour of the second approach. The accuracy of the angles was better than $\pm 5^\circ$. A better result for the second angle could be obtained by rotating the mask into the direction of both axis of the ellipse and convolving again. Using the resulting similarity measure instead of the eigenvalues resulted in an improved accuracy of $\pm 2^\circ$, because the similarity encoded in the eigenvalues of the orientation tensor is often a little bit too small. The results degrade for tilt angles larger than $\pm 60^\circ$ due to the shape of the mask, but this is of no importance for this application.

5. Results

Several "gold standard" data sets have been generated for testing, for example the data shown in Figure 11. There, the vortex characteristics are known and can be compared to the results of our algorithms. In some of these test data, the vortex direction is orthogonal to the image plane, in others it is not. Furthermore, the effects of noise to the results of the algorithms can be studied quite well. The methods presented so far are all pretty robust in terms of noise due to the averaging effect of the convolution. Furthermore, as the masks all have zero mean, the methods are not affected by any mean flow.

Detecting the vortex core with different masks like a pure rotation or a Rankine vortex always gives essentially the same results. Concerning the size of a vortex, a pure rotational mask or Rankine vortex results in diameters which are too large. Here, a modified Rankine vortex gives better results, for first approximations as well as subpixel accuracy. The Rankine vortex was modified by enlarging the velocity at the core radius, or within a small neighbourhood of the core radius, and setting the velocity outside of the core radius to zero. Another rotational mask, where only the velocities at a ring centered at the core radius are larger then zero, behaves similar. To determine the vortex direction, a rotational mask or Rankine vortex in combination with a scalar-valued elliptical mask on the resulting similarity image gives the best results as described in Section 4.3. The methods give really good results even when values like position or size, which have to be determined beforehand for the computation of size or orientation, do not have subpixel accuracy.

After determining the accuracy of the methods, these methods were applied to several of the 3-C PIV images from

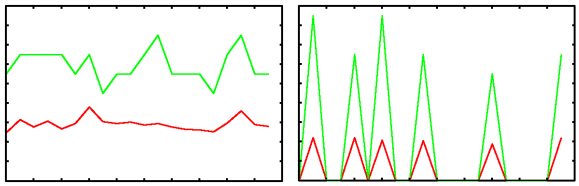

Figure 12: *Similarity (red) and scale (green) of the vortices of 20 images each of two measurement positions. The first position shows a young and well defined vortex (left). At the second position, the vortex is quite old and often, the vortex can not be found at all (right). The x-axis gives the number of the image and the y-axis gives the similarity values in red and the diameter of the vortices in green. The results are computed without orientation correction or subpixel accuracy.*

the HART II test. Some results can be seen in Figures 5, 7, 9, and 12. As the methods are all robust in terms of noise and independent of mean flow, they behave well on this data. The vortex characteristics thus computed can now be used for visualization.

6. Conclusion and Future Work

The authors have investigated several image processing methods based on convolution, integration, bisection, and the orientation tensor, to determine parameters of vortices given by a cut of the vortices with the image plane. Position, size, direction and velocity at the core radius can be determined quite robust and precise with the presented methods, for an accuracy of edge-length as well as subpixel accuracy. The methods are all independent of any mean flow and robust in terms of noise, which is both important for the evaluation of the HART II PIV images. The techniques are applicable to other settings as well, especially the computation of the vortex position. Naturally, the orientation correction is only applicable to perfectly round vortices. For deformed vortical structures, the rest of the methods will only perform as well as for round vortices if the shape is determined beforehand and coded into the masks.

In the future, the authors want to model the interaction between nearby vortices with masks. Furthermore, the whole wake has to be identified and classified. Therefore, the vector fields have to be segmented into several vortices, the mean flow component, and the wake areas with a lot of vorticity but where no vortices have been formed yet.

Acknowledgments

The support of the HART II team, consisting of members from DLR Germany, NASA Langley and US Army AFDD, the French ONERA and the Dutch DNW, is greatly acknowledged. They provided 3C-PIV real world high quality data for analysis and practical application of the methodologies described.

Furthermore, we like to thank the members of the FAnToM development team at the Technical University of Kaiserslautern, and University of Leipzig ,especially Tobias Hilbert and Evi Worf, for their help with programming and production of the pictures.

References

[BBvdW*02] BURLEY C. L., BROOKS T. F., VAN DER WALL B. G., RICHARD H., RAFFEL M., BEAUMIER P., DELRIEUX Y., LIM J. W., YU Y. H., TUNG C., PENGEL K., MERCKER E.: Rotor wake vortex definition - initial evaluation of results of the HART-II study. In *28th EUROPEAN ROTORCRAFT FORUM* (Bristol, England, 2002). 1, 2, 3

[BBvdW*03] BURLEY C. L., BROOKS T. F., VAN DER WALL B. G., RICHARD H., RAFFEL M., BEAUMIER P., DELRIEUX Y., LIM J. W., YU Y. H., TUNG C., PENGEL K., MERCKER E.: Rotor wake vortex definition using piv measurements - corrected for orientation. In *9th AIAA/CEAS Aeroacoustics Conference* (2003). 3, 4

[ES] EBLING J., SCHEUERMANN G.: Fourier transform on multivector fields. *IEEE TVCG*. http://www.informatik.uni-leipzig.de/bsv/Ebling/pdfs/TVCG2004.pdf. 2, 4

[ES03] EBLING J., SCHEUERMANN G.: Clifford convolution and pattern matching on vector fields. In *Proceedings of IEEE Visualization 2003* (Los Alamitos, CA, 2003), IEEE Computer Society, pp. 193–200. 2, 4

[GK95] GRANLUND G. H., KNUTSSON H.: *Signal Processing For Computer Vision*. Kluwer Academic Publishers, Dordrecht, The Netherlands, 1995. 4

[HEWK03] HEIBERG E. B., EBBERS T., WIGSTRÖM L., KARLSSON M.: Three dimensional flow characterization using vector pattern matching. *IEEE Transactions on Visualization and Computer Graphics 9 (3)* (2003), 313–319. 2, 4, 5

[HYWL00] HEINECK J., YAMAUCHI G., WOODCOCK A., L.LAURENCO: Application of three-component piv to a hovering rotor wake. In 56^{th} *Annual Forum of the American Helicopter Society* (Virginia Beach, VA, USA, 2000). 3

[Ran58] RANKINE W.: *Manual of Applied Mechanics*. London, 1858. 3

[RRE*04] RAFFEL M., RICHARD H., EHRENFRIED K., VAN DER WALL B. G., BURLEY C. L., BEAUMIER P., MCALISTER K., PENGEL K.: Recording and evaluation methods of piv investigations on a helicopter rotor model. In *Experiments in Fluids 36* (2004), Springer Verlag, pp. 146–156. 2, 3, 4

[Scu75] SCULLY M.: *Computation of Helicopter Rotor Wake Geometry and It's Influence on Rotor Harmonic Airloads*. Tech. Rep. ASRL TR 178-1, Masachussetts Institute of Technology, March 1975. 3

[Vat98] VATISTAS G.: New model for intense self-similar vortices. *Experiments in Fluids 14 (4)* (1998), 462–469. 3

[vdWBY*] VAN DER WALL B. G., BURLEY C. L., YU Y. H., RICHARD H., PENGEL K., BEAUMIER P.: The HART II test - measurement of helicopter rotor wakes. Elsevier Press. 1, 2, 3